On OFDM and SC-FDE Transmissions in Millimeter Wave Channels with Beamforming

Meng Wu, Dirk Wübben, Armin Dekorsy
University of Bremen, Bremen, Germany
Email:{wu,wuebben,dekorsy}@ant.uni-bremen.de

Paolo Baracca, Volker Braun, Hardy Halbauer
Bell Labs, Nokia, Germany
Email:{paolo.baracca,volker.braun,hardy.halbauer}@nokia.com

***Abstract*—The air interface for millimeter wave (mmWave) communications must be designed by properly taking into account the specific characteristics of the wireless channel at higher frequencies. In this work, we start by considering a channel model recently proposed in the literature for mmWave communications in outdoor urban scenarios. First, on top of this channel model we implement a sectorized beamforming model necessary to compensate the large path-loss at mmWave range and study how channel statistics, namely, delay spread and angle spread, are influenced by employing different beamwidths. Subsequently, adopting this beamforming model in the mmWave channel, orthogonal frequency division multiplexing (OFDM) and single carrier frequency domain equalization (SC-FDE) systems are compared. Extensive link level simulations are performed by considering different beamwidths, line-of-sight (LOS) coverage and channel coding. Numerical results show that SC-FDE using minimum mean square error (MMSE) equalization performs close to OFDM in coded systems. However, SC-FDE might be beneficial in practice due to much lower peak to average power ratio (PAPR) than OFDM.**

I. Introduction

Thanks to the large bandwidth available at high frequencies between 3 GHz and 300 GHz, millimeter wave (mmWave) communications attract increasing interests in achieving highly boosted data rate [1] and is recognized to be a key technology in 5G architectures [2]. To understand the characteristics for wireless transmissions at mmWave range, proper mmWave channel modeling is required. In [3], a 3D mmWave channel model consistent with the 3GPP modeling methodology [4] was presented based on ray-tracing that matches real measurements in New York city [5]. Compared to the 3GPP counterpart, a reduced number of effective clusters has been observed for mmWave links. Additionally, the channel statistics such as delay spread and angle spread were also investigated for omni-directional transmissions. Some further channel models have been presented in [6] and by the MiWEBA project [7] for different outdoor scenarios. Due to the large path-loss at mmWave frequencies, beamforming has to be applied for compensating this performance loss [8], [9]. By using either directional antenna or omni-directional antenna arrays, both transmit and receive signal beams can be steered adaptively to achieve beamforming gains. These beamforming strategies have to be embedded in a complete mmWave channel model. Correspondingly, the channel statistics including beamforming need to be analyzed to facilitate proper air interface design.

In this paper, we consider mmWave mobile communications in outdoor scenarios using the 3D channel model for omni-directional transmissions proposed in [3]. One of our contributions is to build the sectorized beamforming model [8] on top of this channel model and examine the influence of using varying beamwidths on the channel statistics such as delay and angle spread. Moreover, inspired by [10] we initiate link level simulations to study and compare the performance of different air interfaces, namely, orthogonal frequency division multiplexing (OFDM) and single carrier frequency domain equalization (SC-FDE) in mmWave channels with beamforming. Our numerical investigations indicate that SC-FDE performs close to OFDM in coded systems. However, SC-FDE might be advantageous in achieving lower peak to average power ratio (PAPR), while low complex one-tap equalization can still be applied as for OFDM.

The remainder of this paper is organized as follows. In Section II the 3D mmWave channel model proposed in [3] is shortly reviewed. Subsequently, a sectorized beamforming model is presented and built on top of the channel in Section III to combat the large path-loss at mmWave frequencies with examination of the altered channel statistics. Afterwards, performance results from link level simulations are discussed in Section IV for comparing OFDM and SC-FDE in different scenarios, for example, impacts of using different beamwidths and code rates on the system performance are stressed. Finally, some conclusions are given in Section V.

II. 3D Millimeter Wave Channel Model

In this section, the 3D mmWave channel model for the urban micro (UMi) environment at 73 GHz proposed in [3] is briefly recaptured. This model is pioneered by [11] and based on ray-tracing data that matches the measurement setup in New York city [5]. The channel modeling for mmWave communications in cellular networks is especially important in a non line-of-sight (NLOS) environment. Following the approach applied for 3GPP standardization [4], omni-directional antennas for both transmission and reception result in N clusters of received replicas, where each cluster includes L subrays. Each subray is characterized by its time delay, power, azimuth angle of departure (AoD), azimuth angle of arrival (AoA), zenith angle of departure (ZoD), and zenith angle of arrival (ZoA). Following the 3GPP-near channel modeling procedure, the channel impulse response (CIR) is generated

for NLOS mmWave channels. Alternatively, for line-of-sight (LOS) channels a weighted LOS ray is added to the generated NLOS channel at time instant 0 based on the Rician factor K. Specifically, the LOS component is scaled by $\sqrt{K/(1+K)}$ whereas the NLOS channel is scaled by $\sqrt{1/(1+K)}$ to achieve normalized power. More details and specific parameter values can be found in [3].

By generating different large scale parameters, the cumulative distribution function (CDF) of the root mean square (RMS) delay spread and angle spread using the above mmWave channel model for NLOS and LOS environments are obtained and shown in Fig. 1 and Fig. 2, respectively. The transmitter-receiver distance is chosen randomly between $50\,\mathrm{m}$ and $200\,\mathrm{m}$ which affects the ZoD and ZoA bias as they are distance dependent [3].

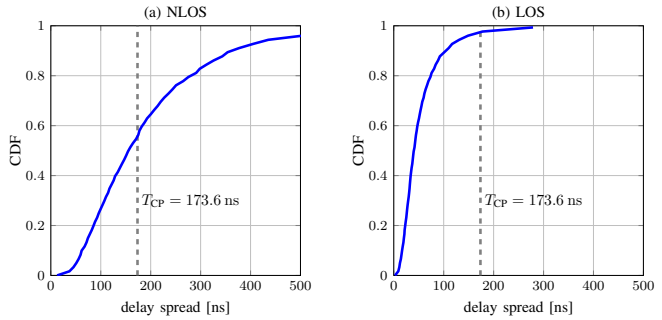

Fig. 1: CDF of delay spread in (a) NLOS and (b) LOS mmWave channels assuming omni-directional transmissions.

It can be observed in Fig. 1 that approximately 95% of the delay spread is concentrated under $500\,\mathrm{ns}$ in the NLOS channel. This is reduced to $200\,\mathrm{ns}$ in the LOS channel. Meanwhile, the median is decreased from $160\,\mathrm{ns}$ to $50\,\mathrm{ns}$. For the discussion in Section IV the duration of the cyclic prefix (CP) $T_{\mathrm{CP}} = 173.6\,\mathrm{ns}$ considered for the OFDM and the SC-FDE systems is indicated. It is implied that beamforming is required to narrow the delay spread due to its wide distribution especially in the NLOS channel, as discussed in Section III.

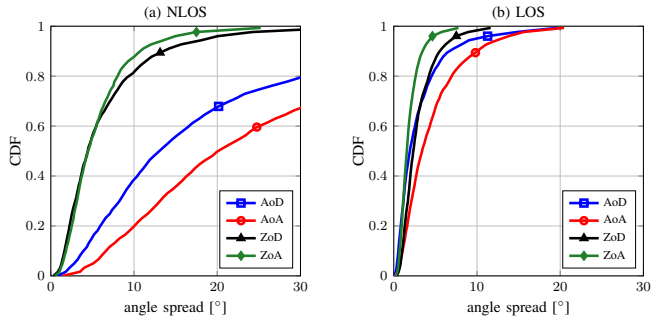

Fig. 2: CDF of AoD, AoA, ZoD and ZoA angle spreads in (a) NLOS and (b) LOS mmWave channels assuming omni-directional transmissions.

On the other hand, the azimuth angle spreads for AoD and AoA are distributed more widely compared to the zenith angle spreads for ZoD and ZoA, as shown in Fig. 2. This is due to the fact that large elevation angles, which are obtained by steering the antenna to the sky and the ground more tendentiously, seldom occur to yield clusters. Furthermore, significantly reduced angle spreads are observed in the LOS channel compared to the NLOS channel.

III. Beamforming

In mmWave communications, beamforming acts as a key technique to compensate the large path-loss at mmWave range. This can be achieved by applying either directional antennas or omni-directional antenna arrays [12]. For simplicity, we employ the sectorized beamforming model presented in [8].

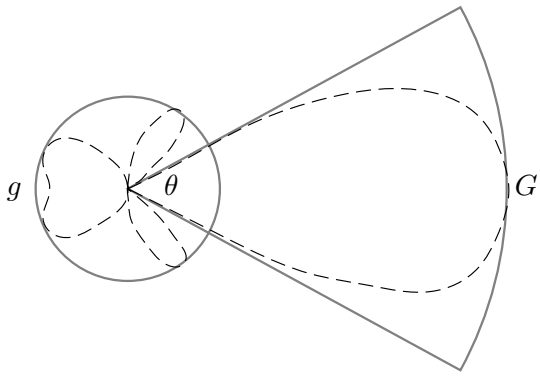

Fig. 3: Sectorized beamforming model specified by constant gain G within beamwidth θ and front-back ratio g/G.

As shown in Fig. 3, this model is characterized by a constant gain G within the beamwidth θ and front-back ratio (FBR) G/g. Typically, the FBR is set to $30\,\mathrm{dB}$. The relation between the gain G and the beamwidth θ in degree is given by [13]

$$G = \frac{32400}{\theta^2}\,. \tag{1}$$

In Tab. I, some typical values of beamwidth θ leading to beamforming gain G are listed. In particular, no gain, i.e., $G = 0\,\mathrm{dB}$, is obtained for omni-directional transmissions. Since a 3D beamforming model is considered here, the beamwidth θ is defined and assumed to be identical in both azimuth and zenith directions. Accordingly, it matches the 3D mmWave channel model presented in Section II. Embedding this beamforming model to the channel is elaborated in the sequel.

θ	omni	$60°$	$30°$	$7°$
G	$0\,\mathrm{dB}$	$9.54\,\mathrm{dB}$	$15.56\,\mathrm{dB}$	$28.2\,\mathrm{dB}$

TABLE I: Exemplary values of beamwidth θ with the corresponding beamforming gain G.

A single stream transmission in a NLOS channel with beamforming at both transmitter and receiver is shown in Fig. 4. The transmitter and receiver beams are firstly steered to point in the direction corresponding to the cluster with the highest power, which is assumed to be located centrally in

the beam. Subsequently, other clusters are checked if they fall into the beam in both azimuth and zenith directions as well at transmitter and receiver side. Those clusters within the beamwidth (solid lines in Fig. 4) benefit from a beamforming gain G, whereas the other clusters (dashed lines in Fig. 4) failing to be in at least one beam in either direction are subject to the FBR.

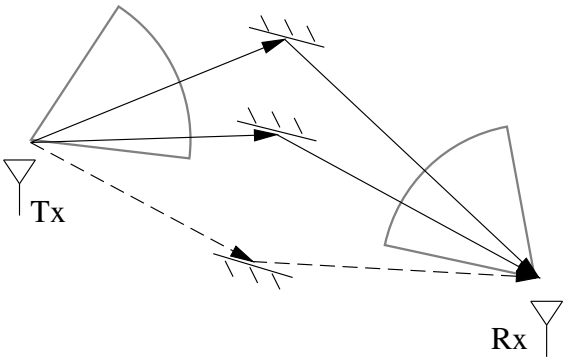

Fig. 4: Beamforming at both transmitter and receiver in a NLOS channel. Pointing both beams to the cluster with the highest power, the clusters falling in the beams (solid lines) benefit from a gain G, whereas the clusters out of at least one beam (dashed lines) are attenuated by the FBR.

The beamforming mechanism presented above can be employed in a LOS channel similarly. In this case, both beams at transmitter and receiver are pointed directly to each other since the LOS ray achieves the most significant gain compared to the NLOS clusters. Depending on the relative angle of these NLOS clusters to the LOS ray, the clusters within both beams achieve the beamforming gain G while FBR leads to further reduced power for the other clusters.

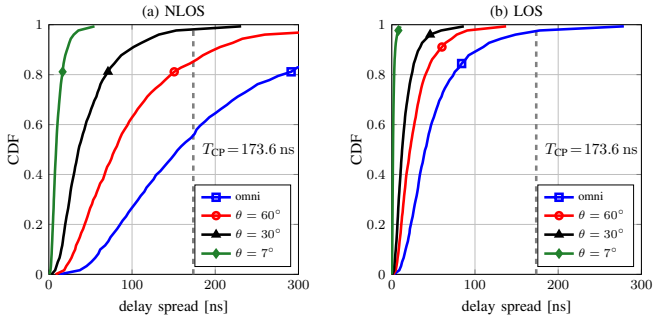

Fig. 5: CDF of delay spread in (a) NLOS and (b) LOS mmWave channels with beamforming of different beamwidths.

The delay and angle spreads in Fig. 1 and Fig. 2 for omni-directional transmissions are re-considered in Fig. 5 - 9 using beamforming with different beamwidths θ as specified in Tab. I. On one hand, smaller beamwidth leads to significantly reduced delay spread as demonstrated already by the measurements in [9]. For example, as can be observed in Fig. 5, with $\theta = 7°$ beamwidth nearly 80% delay spread is constrained under 10 ns in the NLOS channel whereas over 95% delay spread is concentrated within 5 ns in the LOS channel. On the other hand, the angle spreads are improved greatly by

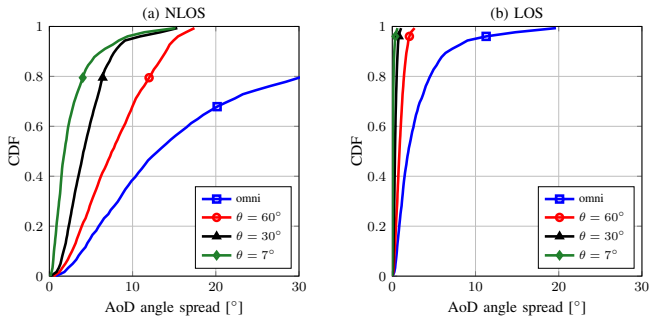

Fig. 6: CDF of AoD angle spread in (a) NLOS and (b) LOS mmWave channels with beamforming of different beamwidths.

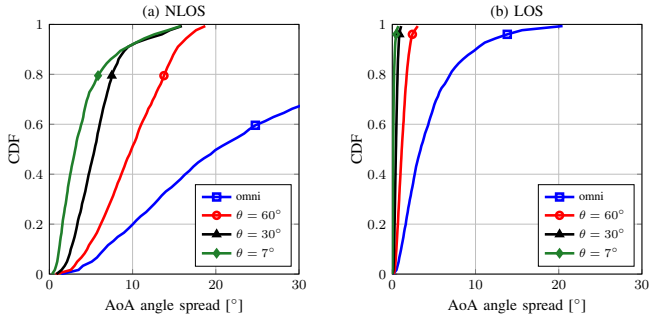

Fig. 7: CDF of AoA angle spread in (a) NLOS and (b) LOS mmWave channels with beamforming of different beamwidths.

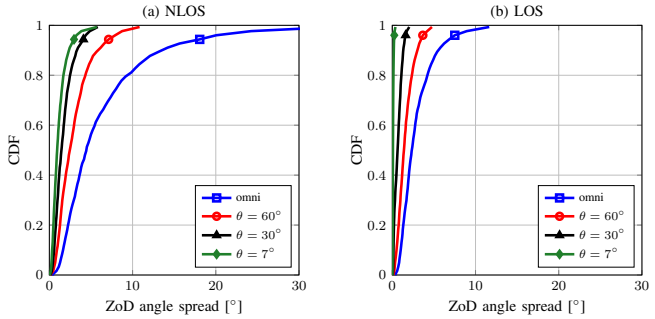

Fig. 8: CDF of ZoD angle spread in (a) NLOS and (b) LOS mmWave channels with beamforming of different beamwidths.

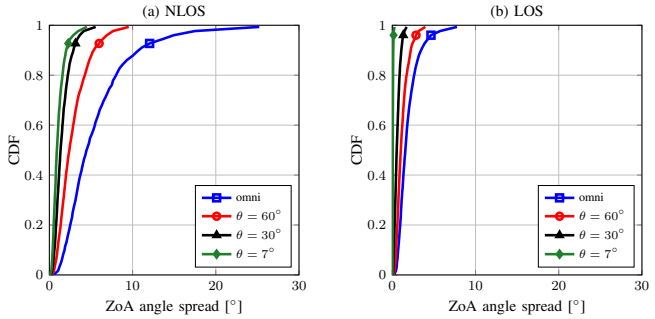

Fig. 9: CDF of ZoA angle spread [°] in (a) NLOS and (b) LOS mmWave channels with beamforming of different beamwidths.

beamforming, especially in the azimuth direction as visualized in Fig. 6 and Fig. 7. For instance, Fig. 7(a) indicates that in case of NLOS, all AoD angle spread is constrained under 20° even for a $\theta = 60^\circ$ beamwidth whereas omni-directional transmission yields only 50% in this case.

IV. Performance Evaluation

A. System Setup and Parametrization

For performance evaluations by link level simulations, the mmWave channel parameters provided in [3] are applied. The numerology for OFDM and SC-FDE transmissions are defined according to the METIS project [14]. Specifically, each data frame contains $N_\mathrm{C} = 2048$ subcarriers with 4-QAM and the subcarrier spacing is set to $720\,\mathrm{kHz}$, resulting in a sampling rate of $1.47456\,\mathrm{GHz}$. We consider a CP overhead of $\beta = 1/8$ leading to a data frame (without CP) duration of $1388.9\,\mathrm{ns}$ and a CP duration of $T_\mathrm{CP} = 173.6\,\mathrm{ns}$. In case of channel coding, an optimized irregular LDPC code of rate R_C is applied with a maximum of 100 iterations for decoding. Each data frame is encoded individually and thus corresponds to one entire codeword, resulting in a constant codeword length of $N_\mathrm{C}\log_2(M) = 4096$. The SNR is defined as $E_b/N_0 = 10\log_{10}\frac{1}{\log_2(M)R_\mathrm{C}\sigma_n^2} - G$ in dB to take into account the impact of modulation alphabet M, code rate R_C and beamforming gain G. Additionally, the mmWave channel is assumed to be perfectly known at the receiver and no hardware impairments are considered. The impact of hardware impairments are investigated in [15].

B. Beamforming

In order to exhibit the impact of beamforming with different beamwidths, the bit error rate (BER) performance for an uncoded OFDM system is shown in Fig. 10.

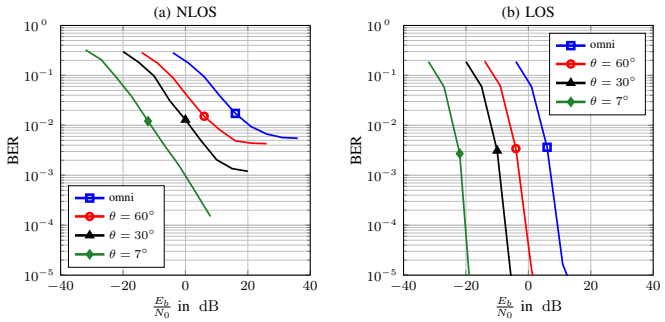

Fig. 10: BER performance in uncoded OFDM systems using beamforming with different beamwidths, (a) for NLOS channel and (b) for LOS channel.

It can be observed that significant gains are achieved by decreasing θ. Furthermore, in NLOS channels error floors occur for large beamwidth θ as the CP is not long enough to achieve inter-symbol interference (ISI) free transmissions. For example, the median delay spread is approximately $160\,\mathrm{ns}$ as shown in Fig. 5(a) using omni-directional antennas whereas the CP length is $T_\mathrm{CP} = 173.6\,\mathrm{ns}$. However, as narrower beamwidths lead to reduced CIR lengths the error floors can be reduced correspondingly. When applying beamforming with $\theta = 7^\circ$, no error floor is observed until BER $= 10^{-4}$. On the other hand, the performance in LOS channels is improved significantly compared to NLOS channels, where error floors also completely disappear even for omni-directional transmissions. This is due to only minor remaining frequency selectivity in the LOS environment as indicated by Fig. 5(b) resulting in reduced ISI power.

C. OFDM vs SC-FDE

In this subsection the BER performance of the OFDM and the SC-FDE system is evaluated for NLOS and LOS channels for beamwidths $\theta = 30^\circ$ and $\theta = 7^\circ$. Fig. 11 shows the BER for uncoded transmissions. As expected, OFDM outperforms SC-FDE with zero forcing (ZF), but the best performance ist achieved by SC-FDE with MMSE equalization as the inherent frequency diversity is inherently exploited also without channel coding. On the other hand, the performance of OFDM is limited by some subcarriers with deep fading. As discussed before, for beamwidth $\theta = 30^\circ$ it is likely that the CIR length exceeds the CP length and the remaining ISI leads to an error floor. For beamwidth $\theta = 7^\circ$ the delay spread is reduced and no error floor is observed here.

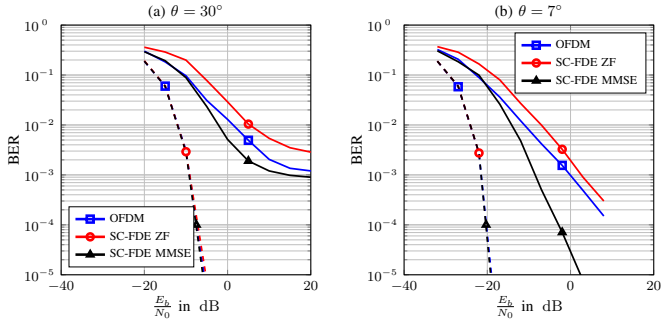

Fig. 11: BER performance in uncoded OFDM and SC-FDE systems using beamforming with (a) $\theta = 30^\circ$ and (b) $\theta = 7^\circ$, NLOS (—) and LOS (- - -) channels.

Fig. 12 depicts the corresponding results with channel coding. Obviously, OFDM achieves now significant gains while the gain for SC-FDE with MMSE equalization is only moderate. It is well-known, that channel coding can exploit the frequency selectivity over different subcarriers in OFDM systems quite well. Contrarily, in case of SC-FDE the equalization in frequency domain leads to an equivalent channel in time domain with averaged channel quality. Correspondingly, the gains achievable by channel coding are limited. In Fig. 12(a) a loss of approximately $1\,\mathrm{dB}$ for SC-FDE with MMSE compared to OFDM is observed. In case of LOS channels, all transmission schemes achieve identical superior performance due to minor frequency selectivity. As demonstrated by Fig. 12(b) almost no difference is observed between OFDM and SC-FDE with MMSE for beamwidth $\theta = 7^\circ$. Furthermore, here the gains achieved by coding are less compared to the gains for $\theta = 30^\circ$. Both observations

are caused by the limited frequency diversity for the narrower bandwidth. Although SC-FDE performs slightly worse than OFDM, it may be preferable in practice because of lower PAPR.

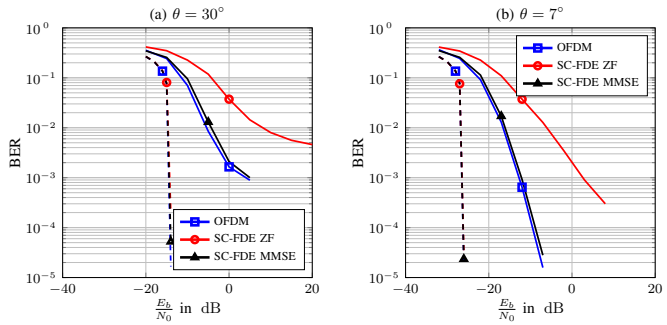

Fig. 12: BER performance in coded OFDM and SC-FDE systems using beamforming with (a) $\theta = 30°$ and (b) $\theta = 7°$, NLOS (—) and LOS (- - -) channels.

D. Impact of Code Rate

The BER performance for coded OFDM and SC-FDE transmissions in NLOS channels are shown in Fig. 13 for a stronger code with $R_C = 0.25$ and a weaker code with $R_C = 0.75$. It is shown that OFDM performs even identically as SC-FDE with MMSE for $R_C = 0.75$. Moreover, the gain by OFDM over SC-FDE with MMSE observed in Fig. 12 for $R_C = 0.5$ is slightly enlarged by the stronger code with rate $R_C = 0.25$. This is attributed to the fact, that the stronger channel code is able to exploit more gains from frequency selectivity. Due to this reason, also the error floor observed for beamwidth $\theta = 30°$ in Fig. 12(ac) is lowered by applying the stronger code.

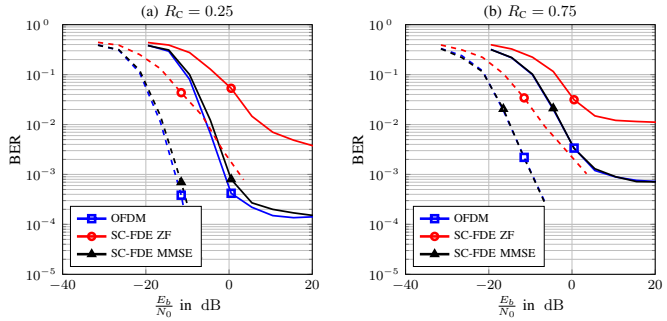

Fig. 13: BER performance in coded OFDM and SC-FDE systems for NLOS channel using beamforming with code rate (a) $R_C = 0.25$ and (b) $R_C = 0.75$ with $\theta = 30°$ (—) and $\theta = 7°$ (- - -).

V. Conclusion

In this paper, a 3D channel model from the literature consistent with the 3GPP modeling methodology is adopted for millimeter wave communications with a sectorized beamforming model built on top of it. It is shown that besides the beamforming gain, the delay and angle spreads are reduced significantly by employing narrower beamwidths. Furthermore, OFDM and SC-FDE systems are examined and compared on mmWave links using the presented channel model with beamforming. As a result, SC-FDE with MMSE is shown to perform close to OFDM in coded systems but may be preferable in practice due to lower PAPR. The work presented here is extended to the investigation of hardware impairments caused by phase noise, IQ imbalance, non-linear power amplifiers, and limited quantization resolution for OFDM and SC-FDE in [15].

References

[1] Z. Pi and F. Khan, "An Introduction to Millimeter-Wave Mobile Broadband Systems," *IEEE Communications Magazine*, vol. 49, no. 6, pp. 101–107, Jun. 2011.

[2] S. G. Larew, T. A. Thomas, M. Cudak, and A. Ghosh, "Air Interface Design and Ray Tracing Study for 5G Millimeter Wave Communications," in *IEEE Globecom Workshops - Emerging Technologies for LTE-Advanced and Beyond-4G (GC'13 Wkshps)*, Atlanta, GA, USA, Dec. 2013.

[3] T. A. Thomas, H. C. Nguyen, G. R. MacCartney, and T. S. Rappaport, "3D mmWave Channel Model Proposal," in *IEEE 80th Vehicular Technology Conference (VTC'14-Fall)*, Vancouver, Canada, Sept. 2014.

[4] *Study on 3D Channel Model for LTE (Release 12)*, 2014, TR 36.873 V1.3.0.

[5] T. S. Rappaport, G. R. MacCartney, M. K. Samimi, and S. Sun, "Wideband Millimeter-Wave Propagation Measurements and Channel Models for Future Wireless Communication System Design (Invited)," *IEEE Transactions on Communications*, vol. 63, no. 9, pp. 3029–3056, Sept. 2015.

[6] E. Torkildson, H. Zhang, and U. Madhow, "Channel Modeling for Millimeter Wave MIMO," in *Information Theory and Applications Workshop (ITA,10)*, San Diego, CA, USA, Jan. 2010.

[7] EU FP7 MiWEBA, "Deliverable D5.1: Channel Modeling and Characterization," Jun. 2014.

[8] T. Bai, A. Alkhateeb, and R. W. Heath, "Coverage and Capacity of Millimeter-Wave Cellular Networks," *IEEE Communications Magazine*, vol. 52, no. 9, pp. 70–77, Sept. 2014.

[9] G. R. MacCartney, T. S. Rappaport, and M. K. Samimi, "Exploiting Directionality for Millimeter-Wave Wireless System Improvement," in *IEEE International Conference on Communications (ICC'15)*, London, UK, Jun. 2015.

[10] A. Ghosh, T. A. Thomas, M. C. Cudak, R. Ratasuk, P. Moorut, F. W. Vook, T. S. Rappaport, G. R. MacCartney, S. Sun, and S. Nie, "Millimeter-Wave Enhanced Local Area Systems: A High-Data-Rate Approach for Future Wireless Networks," *IEEE Journal on Selected Areas in Communications*, vol. 32, no. 6, pp. 1152–1163, Jun. 2014.

[11] M. R. Akdeniz, Y. Liu, M. K. Samimi, S. Sun, S. Rangan, T. S. Rappaport, and E. Erkip, "Millimeter Wave Channel Modeling and Cellular Capacity Evaluation," *IEEE Journal on Selected Areas in Communications*, vol. 32, no. 6, pp. 1164–1179, Jun. 2014.

[12] V. Rabinovich and N. Alexandrov, *Antenna Arrays and Automotive Applications*, Springer Verlag, 2013.

[13] Z. Pi and F. Khan, "A Millimeter-Wave Massive MIMO System for Next Generation Mobile Broadband," in *46th Asilomar Conference on Signals, Systems and Computers (Asilomar'12)*, Pacific Grove, CA, USA, Nov. 2012.

[14] *Components of a New Air Interface - Building Blocks and Performance*, Apr. 2014, D2.3, METIS.

[15] M. Wu, D. Wübben, A. Dekorsy, P. Baracca, V. Braun, and H. Halbauer, "Hardware Impairments in Millimeter Wave Communications using OFDM and SC-FDE," in *20th International ITG Workshop on Smart Antennas (WSA 2016)*, Munich, Germany, Mar. 2016.